SEIS MICA

Seismoacoustic measurements of the OSIRIS-REx re-entry with an off-grid Raspberry PiShake

Benjamin Fernando [ID] * [1], **Constantinos Charalambous** [ID] [2], **Christelle Saliby** [ID] [3], **Eleanor K. Sansom** [ID] [4], **Carene Larmat** [ID] [5], **David Buttsworth** [ID] [6], **Daniel C. Hicks** [7], **Roy Johnson** [ID] [8], **Kevin Lewis** [ID] [1], **Meaghan McCleary** [ID] [9], **Giuseppe Petricca** [ID] [10], **Nick Schmerr** [ID] [11], **Fabian Zander** [ID] [6], **Jennifer Inman** [ID] [9]

[1]Department of Earth and Planetary Sciences, Johns Hopkins University, Baltimore, Maryland, United States, [2]Department of Electrical and Electronic Engineering, Imperial College London, London, United Kingdom, [3]Université Côte d'Azur, Observatoire de la Côte d'Azur, CNRS, IRD, Géoazur, Valbonne, France, [4]School of Earth and Planetary Science, Curtin University, Perth, Australia, [5]Los Alamos National Laboratory, New Mexico, United States, [6]Institute for Advanced Engineering and Space Sciences, University of Southern Queensland, Queensland, Australia, [7]United States Department of Defence (KBR Consultant), Las Cruces, New Mexico, United States, [8]NASA Ames Research Center, Moffett Field, California, United States , [9]NASA Langley Research Center, Hampton, Virginia, United States, [10]Raspberry Shake, S.A., Panama, [11]Department of Geology, University of Maryland, College Park, Maryland, United States

Abstract   Hypersonic re-entries of spacecraft are valuable analogues for the identification and tracking of natural meteoroids re-entering the Earth's atmosphere. We report on the detection of seismic and acoustic signals from the OSIRIS-REx landing sequence, acquired near the point of peak capsule heating and recorded using a fully off-grid Raspberry PiShake sensor. This simple setup is able to record the salient features of both the seismic and acoustic wavefields, including the primary shockwave, later reverberations, and possible locally induced surface waves. Peak overpressures of 0.7 Pa and ground velocities of 2×10^{-6} m/s yield lower bound on the air-to-ground coupling factor between 3 and 44 Hz of 1.4×10^{-6} m/s/Pa, comparable to results from other re-entries.

1 Introduction

1.1 Seismoacoustic measurements of hypervelocity re-entry

Seismic and acoustic measurements are invaluable tools for identifying and locating meteoroids entering the Earth's atmosphere (Edwards et al., 2008). Unlike optical techniques, seismoacoustic techniques allow over-the-horizon measurements to be made, and can continue to track bolides during their dark-flight phase.

The entry, descent, and landing (EDL) of artificial spacecraft can serve as an analogue for these natural meteoroid events, enabling calibration of seismoacoustic measurements using an object of known trajectory, mass, and dimensions (Silber et al., 2023).

However, very rarely do re-entering spacecraft approach velocities representative of naturally-occurring meteorites (>11 km/s, Ceplecha et al., 1998). The exceptions to this are capsules re-entering on interplanetary (as opposed to de-orbital) trajectories.

Such encounters are extremely rare, having occurred only four times on Earth. Sample return capsules from the Genesis (ReVelle et al., 2005), Stardust (ReVelle and Edwards, 2007), Hayabusa (Yamamoto et al., 2011), and Hayabusa2 (Sansom et al., 2022) missions underwent EDLs at around 12 km/s, on the lower end of the velocity distributions of natural meteoroids, though still somewhat representative.

In each case, seismic and acoustic measurements enabled information about the capsule's hypersonic dynamics and the propagation of the sonic boom shockwave to be collected. Ironically, these EDL events are much more common on other planets visited by human spacecraft, but only one has been (unsuccessfully) instrumented (Fernando et al., 2021, 2022).

1.2 The OSIRIS-REx Entry, Descent, and Landing Sequence

The OSIRIS-REx (ORX) sample return capsule was scheduled to re-enter the Earth's atmosphere at 14:41:55 UTC on 2023-09-24, carrying samples from asteroid Bennu (Lauretta et al., 2017). Its atmospheric interface was expected to occur off the coast of San Francisco, California, at an altitude of ∼133 km and a velocity of

---

*Corresponding author: bfernan9@jh.edu

approximately Mach 25 (43,000 km/h; 11.9 km/s).

ORX's heat shield was expected to experience peak frictional heating from the atmosphere (∼3100 K) at a speed of Mach 30 (39,000 km/h; 10.8 km/s) ∼62 km above northern Nevada around 14:42:45 UTC, before continuing downrange to a soft landing at the Dugway Proving Ground in Utah at 14:55 UTC (Ajluni et al., 2015).

1.3 Project aims

This project aimed to co-locate a seismoacoustic station with an optical tracking station close to the point of peak heating, in order to study the re-entry process at the point where the maximum amount of kinetic energy is being dissipated into the atmosphere. Exact co-location of acoustic and seismic measurements enables estimation of coupling parameters across the surface interface, helping to constrain how incident acoustic signals produce their seismic counterparts. This is particularly useful when detecting natural meteoroids given that the worldwide seismic network is much denser than its acoustic equivalent.

Whilst other instrumentation campaigns were planned to record seismic and acoustic signatures using more conventional deployments, these were not co-located with an optical tracking station (Silber et al., 2023).

The nearest permanent seismic station was 50 km away (NN.Q11A at Duckwater, Nevada), precluding the use of an existing seismic network to provide local data. Similarly, no permanent infrasound stations were located nearby. Further constraints were imposed on this deployment by the absence of mains power or wired data connections at the optical tracking sites and the stipulation that the data be live-streamed in real-time over the internet for education and outreach purposes.

Our identified solution was to use a low-cost Raspberry PiShake seismic and infrasound sensor[1] coupled to a portable generator and satellite internet connection to fulfil these aims.

In this paper we present the methodology and initial results from this project, whilst also exploring the scalability of a network of this type. For temporary deployments where real-time data access is required (e.g. for monitoring or triggering purposes) in remote areas, such a configuration may serve as a template. This is especially true for phenomena like EDLs where dense instrument spacings are of interest, and the co-location of seismic and acoustic sensors on a single instrument offers both logistical and processing advantages.

This work builds on previous use of distributed off-grid sensors for seismic sensing (e.g. Kong et al. (2016)) and past incorporation of PiShakes into seismic networks (Winter et al., 2021; Mikael, 2020; Manconi et al., 2018; Lecocq et al., 2020). However, it is the first example of which we are aware of a direct PiShake-satellite connection.

---

[1]Raspberry Shake & Boom, https://manual.raspberryshake.org/boom.html

2 Methodology

2.1 Location

The location of the optical tracking station with which the PiShake (station code: 'RD04A') was co-located was selected by NASA's Scientifically Calibrated In-Flight Imagery (SCIFLI) Team to be close to the point of peak heating in the ORX EDL trajectory, whilst also being remote and far from any artificial light sources.

The selected location was in Eureka County, Nevada (39.264605°N, 116.026934°W), at an elevation of 1843 m AMSL. This site was ∼40.5 km laterally offset from the closest point on the nominal EDL trajectory at a bearing of 199° (meaning the minimum source-receiver distance was expected to be 72.2 km). A schematic illustration of the projected EDL trajectory is shown in Fig. 1. Note that the lateral offset was chosen to enable a reduced slewing rate across the sky for the optical tracking instruments.

A range of hills with peaks up to 2900 m (700 m prominence) to the north and north-east at a range of 5-10 km were also noted.

The chosen site was a flat, dry bed, which was identified as having a surface of unconsolidated alluvium. A small section of the ground was artificially brushed clean and smoothed before the seismometer was deployed. P-wave speeds in unsaturated northern Nevada alluvium are reported in the literature as varying between 365 and 1035 m/s (Allander and Berger, 2009).

At a location this distance from and altitude below the EDL track, we anticipated detection both of the direct sonic boom (on the acoustic sensor) and the induced deformation of the ground (on the seismometer). It was also expected from published literature analysing conventional explosive sources that further features might be detected in the seismic coda, for example coupled surface waves (Novoselov et al., 2020; Langston, 2004). Previous work indicates that these observations are site-specific and hence not a given, with a dependence on both local ground properties and current atmospheric conditions (Wills et al., 2022; Chen et al., 2023).

2.2 Weather

The nearest weather station to the seismometer deployment was at Eureka Airport (39.600506°N, 116.006467°W). The distance between the PiShake location and the airport point is 37.4 km, at a bearing of 2.7° from north. A weather measurement was made at the airport at 14:53 UTC, around 11 minutes after the expected overflight of the capsule.

The recorded air temperature was 8.9°C, with a dewpoint of -1.7°C and a resulting relative humidity of 47%. Barometric pressure was 1022.1 hPa, and the windspeed was recorded as 2.1 m/s from an origin bearing 210°. The resulting surface sound speed is calculated to be 337 m/s.

2.3 Setup

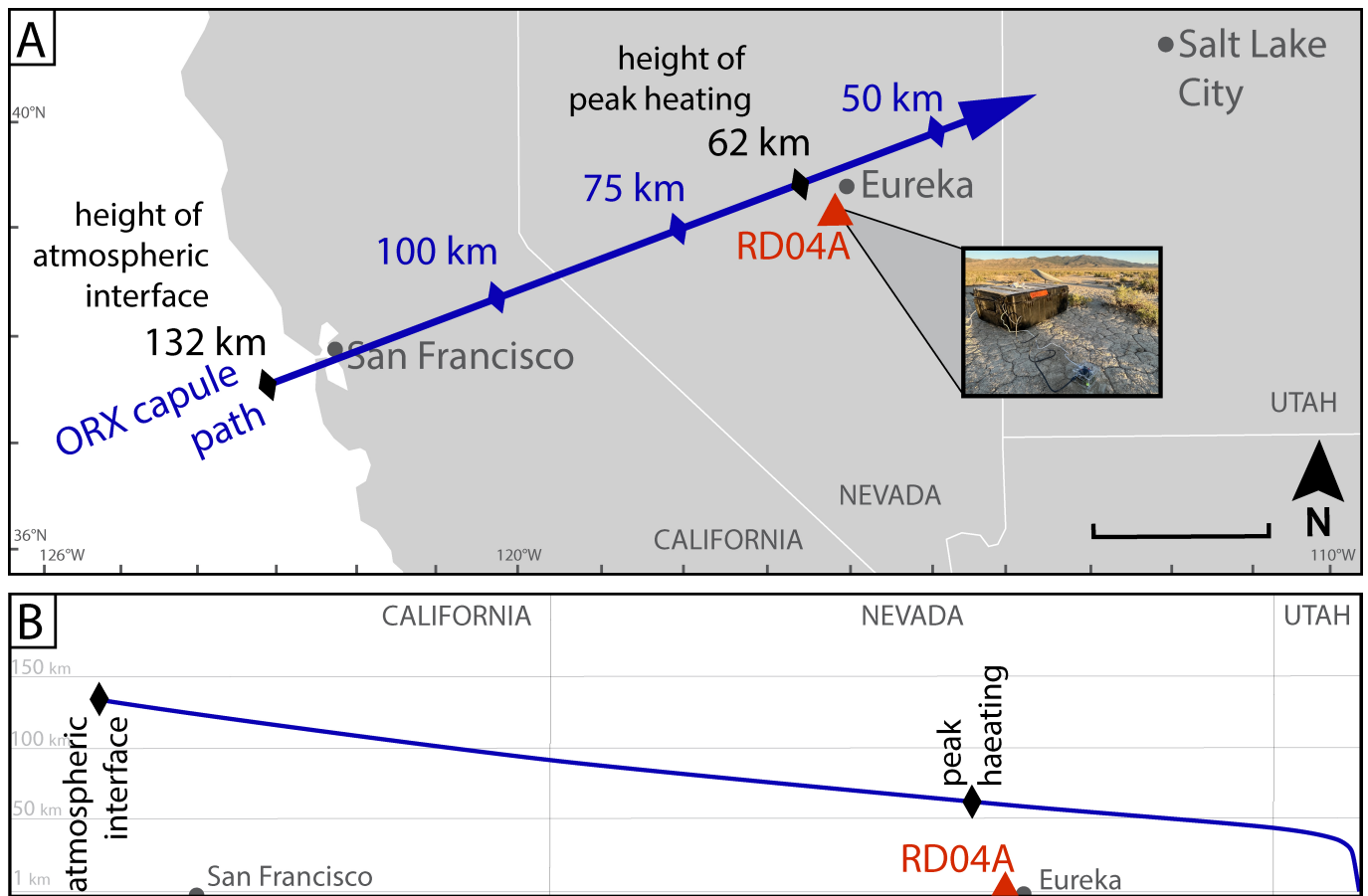A PiShake 'Shake and Boom' equipped with an infrasound sensor and vertical component geophone was

Figure 1 Schematic views of the pre-landing projected ORX EDL path in blue, showing top-down (upper panel) and side-on (lower panel) views. Capsule heights above sea level are indicated along the trajectory. The total length of the path flown after atmospheric interface is approximately 1500 km.

used in this experiment. The instrument was levelled on the ground but not rotationally oriented due to the absence of horizontal component geophones. This setup is shown in Fig. 2. Due to the soil conditions, the sensor could not be feasibly anchored into the ground and simply rested on the surface.

Both the acoustic and seismic sensors sampled using default settings, at 100 samples/second with an estimated bandwidth of -3dB between 0.7 and 44 Hz in velocity for the geophone and -3dB between 1 and 44 Hz for the infrasound sensor.

The sensor was powered by connection to a portable generator approximately 12 m away, which was shielded by makeshift acoustic baffles (bins and camping chairs). A direct connection into a Starlink terminal provided real-time access to the data and livestreaming capability over the PiShake website. Due to the lack of multiple ethernet ports on the terminal, instrument configuration to update metadata could not be done on-site and was executed remotely.

Timing was executed via the instrument's default NTP over the Starlink connection. Data collected between 14:00 and 15:00 UTC is considered reliable, and the background noise levels are representative of the environmental conditions; data are available from before 14:00 UTC on the day of landing but are contaminated by noise from the site setup.

Figure 2 Instrument setup. The PiShake is visible as the transparent box in the foreground, with the geophone and infrasound sensor mounted within the same instrument and levelled using the built-in spirit level. Power (white cable) and data (black cable) are routed through the weatherproof black box. The generator and acoustic baffles are not shown, but the Starlink connection is visible in the background. The unconsolidated alluvial surface and range of hills with peaks 5-10 km away are also visible. Image direction: north (toward EDL trajectory).
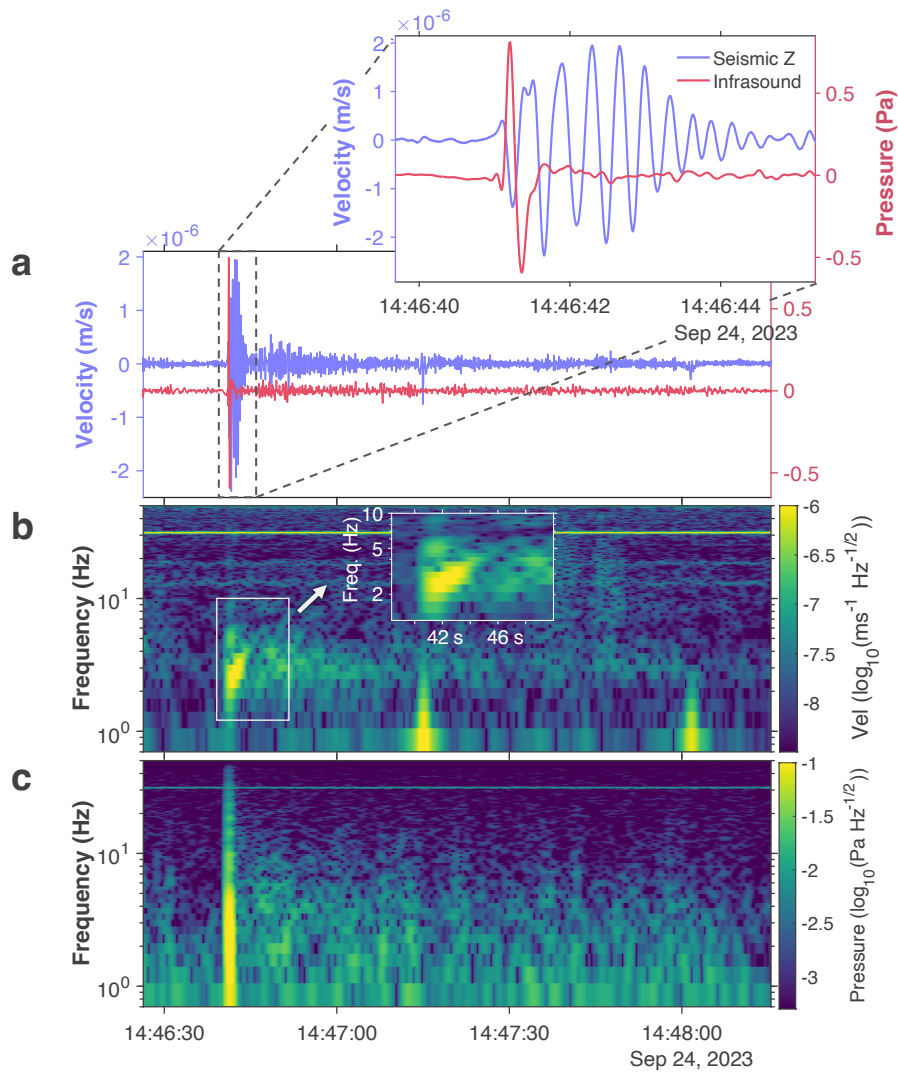
Figure 3 (a) Traces of the seismic (blue) and acoustic (red) data, inset is a detail of the first arrivals. (b) Spectrogram of the seismic data, inset shows a detail of the seismic chirp observed which lasts around four seconds and is dispersive. Bright, vertical spikes at 14:47:15 and 14:48:00 UTC are glitches in the system electronics. Horizontal lines are resonances produced by the generator. (c) Acoustic data, showing a single impulsive arrival at 14:46:45 UTC with no clear coda, but potentially elevated noise levels post-arrival.

3 Results

Pre-landing estimates suggested that any sonic boom would likely arrive at the deployment location around 240 seconds (4 minutes) after the point of peak heating or around 14:46:45 UTC.

Data from the seismic and acoustic instruments are shown in Fig. 3. A sharp peak in both datasets, elevated significantly above the background noise, is recorded at 14:46:41 UTC. This sound was also recorded by the ground team as a loud 'popping' noise at 14:46:45 UTC ± 00:00:03; extremely short in duration and lacking any discernible internal structure or audible rumbling.

As best as could be determined by the ground team, this boom originated from the north of the observation station (toward the EDL trajectory), but from the direction of the horizon rather than from an elevated angle. We attribute this observation to the fact that the capsule is not behaving as a point source. Rather, it behaves as an elongated cylindrical source producing a conical shock with a hyperbolic footprint on the ground.

We note that the arrival time of the sonic boom was in very close agreement with our pre-landing prediction. However, we expect that this degree of agreement is not particularly consequential (i.e., cannot be used to confirm that the EDL trajectory was totally nominal), as our pre-landing estimate of the boom propagation time was linear and neglected atmospheric refraction of the shockwave.

3.1 Infrasound data

The infrasound signal displays rounded 'N-wave' behaviour expected of a downward-propagating sonic boom (Plotkin, 2002), with a rapid overpressure (0.7 Pa) pulse and sharp peak followed by an underpressure trough (0.6 Pa) lasting approximately 0.5 s total.

This shape is characteristic of a shockwave which has been distorted by propagation through a turbulent atmosphere (Pierce and Maglieri, 1972). It is very similar to previously recorded signals from hypersonic re-entries (e.g. ReVelle et al., 2005). Hence, we conclude

that the main infrasound signal is the direct detection of the sonic boom from the capsule and not an acoustic reflection (echo) or rumbling produced by the incident acoustic wave upon the ground.

The background infrasound noise level appears to be slightly enhanced at low frequencies (<10 Hz) following the arrival as compared to before, though not enormously so (Fig. 3, ∼5 s before and after the infrasound arrival). This feature may be the signature of a low-frequency sub-audible infrasonic rumble or may simply be associated with elevated wind noise.

3.2   Seismic data

The seismic dataset appears to be considerably richer than the infrasound signature, with a signal lasting approximately 120 seconds (2 minutes). The first seismic arrival is exactly coincident with the infrasound arrival. This likely represents the shaking of the surface induced by the overpressure (Ben-Menahem and Singh, 1981).

This conclusion is also supported by the polarity of the signal, with the downward motion at first arrival corresponding to the displacement downward of the sensor and ground in response to the acoustic overpressure. Peak shaking of $2x10^{-6}$ m/s is observed, with the boom itself lasting approximately 5 seconds.

The complex coda is likely to have multiple origins, including the excitation of surface waves (Cook et al., 1972), scattering of the shockwave in the atmosphere (Garcia et al., 2022), reflections of the direct shockwave off of topography (Emmanuelli et al., 2021) and of the transmitted shockwave off sub-surface geological features, and the gradual restoration of the equilibrium surface position following compliance-induced deformation.

A short, dispersive, chirp-like signal is apparent between approximately 1 and 7 Hz in the 3-4 seconds following the initial seismic arrival (see inset spectrogram, beginning at 14:46:41 UTC), with higher frequencies arriving later than lower ones. Two potential chirping structures are also observed later in the data (around 14:46:46 and 14:46:50 UTC), though at much lower signal-to-noise ratios.

'Normal' dispersion in chirp structures is indicative of higher frequencies propagating more slowly than lower ones. Such behaviour would be expected for seismic surface waves propagating in the uppermost layers of the ground, where the gradient in sound speed with depth is significant on the scale of the seismic wavelength. Because these surface phases do not arrive before the initial boom, we conclude that they are produced locally to the receiver; as seismoacoustic coupling in the far-field directly below the ORX trajectory would likely see coupled surface waves 'overtaking' the boom due to the higher propagation speeds in the ground.

Similar features, identified as Airy waves, are seen during the Stardust EDL by Edwards et al. (2007), whilst Novoselov et al. (2020) identify Stoneley waves in seismic coda generated by seismoacoustic coupling. These propagate in the thin, low-velocity surface layers where the shear velocity approaches the acoustic wavespeed in air (Wills et al., 2022). This is comparable to the geological setting here, with the PiShake sensor resting on a low-velocity alluvial layer.

3.3   Air-to-ground coupling

The co-location of seismic and acoustic instruments allows us to estimate the ground compliance (the ground's response to the pressure loading from the shockwave at the surface (Sorrells, 1971; Kenda et al., 2020). A number of physical phenomena contribute to the compliance, here we consider the inertial effects originating from the continuity of normal stress and displacement at the ground surface. We note that measurements of seismoacoustic coupling strength are in general very sensitive, in particular to the frequency bands considered, surface topography, and wavefront shape/incident angle (Matoza and Fee, 2014; Bishop et al., 2022).

We estimate the inertial effects by considering how the vertical deformation recorded by the seismometer is related to the surface overpressure. The ground is modelled as a homogeneous, isotropic half-space and the shockwave is modelled as a planar wave. Following Kenda et al. (2020), the compliance K_v is then:

$$K_v = 2c\frac{1 - \nu^2}{E}, \tag{1}$$

where E is the Young's modulus, ν is the Poisson ratio, and c is the advection speed of the pressure loading.

We choose elastic properties for the subsurface corresponding to canonical values for soft superficial alluvium, with V_p = 585 m/s and V_s = 350 m/s, ν = 0.22, and E = 0.4488 MPa. These are commensurate with detailed surveys from the wider region (Allander and Berger, 2009). Local variations in these values may be substantial, but would require a full geophysical survey to better constrain.

These values lead to a compliance dependent on the advection speed c of:

$$K_v = 4.23x10^{-9}c \ \text{m/s/Pa} \tag{2}$$

As we expect the shockwave to propagate at or faster than the speed of sound, we use a value for the advective speed c of 337 m/s, as derived in Sec. 2.2. This is very much a lower limit, as the actual speed of the shockwave is not simple to measure. We also note that this value is much faster than conventional derivations of the compliance, which use wind-driven ground deformation as a source (c ∼2 m/s in Kenda et al., 2020).

These parameters yield a minimum value for the ground compliance of $1.4x10^{-6}$. This gives us a calculated minimum value for the air-to-ground coupling of $4x10^{-6}$ m/s/Pa, using the vertical component of the velocity only.

This value is comparable to that derived from the Stardust EDL by Edwards et al. (2007) of 7.3± $0.2x10^{-6}$ m/s/Pa, which used a similar capsule and trajectory but required a far more complex deployment to estimate.

3.4 Seismoacoustic noise

For completeness, we comment on a number of seismoacoustic noise sources which are apparent in the wider dataset.

Strong resonances in both instruments are observed at 30 Hz, with weaker resonances in the seismic data at ∼11 Hz and ∼19 Hz. These appear as horizontal lines in Fig. 3. These are identified as coming from the generator, and over a longer timescale (not shown here), they display subtle changes in frequency as the generator load varies with changes in the power demand of the optical tracking instruments.

Occasional spikes in the seismic power are also observed, for example at 14:46:45 UTC. These are also thought to be electromagnetic glitches associated with rapid changes in the generator's load. These appear as vertical spikes lines in Fig. 3. One glitch at 14:47:15 UTC partially overprints the seismic coda, though well beyond the point at which the identified surface wave phases have dropped below the noise floor.

4 Discussion

4.1 Scientific utility

This deployment demonstrated the ability of a fully off-grid Raspberry PiShake 'Shake and Boom' sensor to capture valuable data from a transient seismoacoustic event, whilst also making said data publicly accessible via livestream.

Whilst naturally limited in sensitivies to long periods (lower than 1 Hz), this work also demonstrates the ability of the PiShake instrument to capture many of the notable features in the wavetrain, from the initial rounded N-wave to the coda likely associated with Stoneley waves propagating in the low-velocity subsurface. Whilst our single station does not offer the same seismic insight as arrays or co-located broader spectrum instruments would, these features of the wavetrain are recorded comparably to past studies (e.g. ReVelle et al., 2005; ReVelle and Edwards, 2007).

These include the primary shockwave (0.7 Pa overpressure and $2x10^{-6}$ m/s peak ground velocity), an extended seismic coda, and possible air-to-ground surface wave phases. We derive a lower bound on the air-to-ground coupling ratio of $4x10^{-6}$ m/s/Pa, comparable to previous capsule re-entries.

4.2 Deployment suggestions

The use of a surface instrument which is locally powered and not hard-coupled to the ground obviously brings with it disadvantages, not least of which is the generator noise apparent on both sensors. For those looking to undertake similar deployments, we also make the following suggestions:

- The addition of a wind cover to the instrument would likely substantially reduce the noise levels of both the acoustic and seismic data.

- Better anchoring of the instrument into the ground would be expected to especially benefit the seismic data.

- The use of a well-tuned and lubricated generator can minimise the amount of acoustic noise produced, enabling data to be recorded with higher fidelity. A rechargable battery or solar panel would of course decrease noise levels even further.

- A dedicated instrument power supply (whether battery or generator) can avoid fluctuations in the generator load which lead to variations in the generator resonant frequencies. Such variations make removal of the generator noise harder.

- For standard Starlink terminals, the single ethernet output port means that LAN configuration of the instrument must be modified, i.e. it is not possible to connect a laptop and a PiShake to the terminal simultaneously without additional hardware. This can be avoided by connecting the PiShake through a laptop to enable metadata edits, or configuring location and elevation parameters on a different network prior to deployment.

4.3 Scaling to larger arrays

The nominal data uplink rate from a Raspberry Pi Shake&Boom sensor of this type is approximately 2.8 kb/s. A standard Starlink connection comes with a minimum expected data rate of 5 Mb/s. As such, data volumes are unlikely to prove problematic for realistic array sizes (<1000 instruments). We again note, however, that additional hardware would be required to enable multiple wired uploads through a Starlink connector due to the single ethernet port on the terminal.

The power requirements of the sensor are at least 5.0 V DC at 2.5 A, for an electrical power of 12.5W. As such, an intermediate-sized array (∼100 instruments) could likely be powered from a single generator for a number of hours. For signals such as those discussed in this paper, that is likely to be more than sufficient.

Finally, we suggest the co-location of 3D PiShakes with PiShake infrasound sensors would also be advantageous, enabling the the air-to-ground coupling factor to be more robustly estimated as all three components of ground displacement can be considered. A larger array would also enable a more realistic estimation of the shock velocity.

5 Conclusions

We have demonstrated that a fully off-grid, livestreaming Raspberry PiShake sensor was able to capture the notable seismic and acoustic features within the waveforms produced by the OSIRIS-REx EDL sequence. A classical rounded 'N-wave' was recorded by the acoustic sensor (peak overpressure 0.7 Pa), and the reverse polarity signal was recorded by the seismometer (peak downward ground velocity $2x10^{-6}$ m/s), indicating the recording of a sonic boom impacting the

ground with an acoustic coupling of at least 4×10^{-6} m/s/Pa.

No unambiguous acoustic coda is recorded, though a possible detection of low-frequency rumbling is made. An extended seismic coda of more complex origin is also recorded, and lasts several minutes.

Although the initial configuration required substantial bespoke setup with satellite internet and data connections, the marginal cost or challenge of adding extra instruments was small. As such, we believe there is substantial potential for low-cost arrays of this type to be scaled to larger sizes when there is a scientific need to record seismoacoustic phenomena at high SNR in remote locations. Such potential has already been demonstrated with conventional seismometers (Busby and Aderhold, 2020) but not to our knowledge with PiShake-type arrays.

6 Environmental impact

As part of efforts to make scientific research more environmentally accountable and sustainable, we have estimated the 'carbon cost' (expressed as tCO_2e) directly associated with this paper. As is common with such projects, scope definition is challenging. Therefore, we focus on carbon costs directly attributed to this project (i.e., those which would not have otherwise been incurred). We exclude background costs such as the instrument manufacture.

We estimate the total equivalent CO_2 burden of this work at approximately 1.0 tCO_2e, made up of:

- 0.5 tCO_2e associated with a round-trip flight from Baltimore, Maryland to Salt Lake City, Utah; in economy class as estimated by the IATA CO_2 connect calculator [2]

- 0.5 tCO_2e associated with driving an SUV off-road field vehicle from Salt Lake City, Utah to the field site near Eureka, Nevada (approximately 800 miles total); estimated using the US EPA Equivalencies Calculator [3]. Note that this ride was shared by several other instrument groups, we quote here the total cost.

- A negligible amount (<0.01 tCO_2e) produced by running the gasoline-powered generator for one hour.

The above values are estimates only, and we note that differences between calculation methodologies can be substantial.

Acknowledgements

Data and code availability

PiShake data are available freely online from the Raspberry Shake Data Centre and may be accessed via the FDSN (http://www.fdsn.org/datacenters/detail/RASPISHAKE/).

The relevant station code is RD04A with channels EHZ (vertical-component geophone) and HDF (infrasound). Note that the current station location may display as Baltimore, Maryland, where this instrument lives on a more permanent basis. Response removal and other useful tools can be found on the PiShake website at https://manual.raspberryshake.org/metadata.html#example-obspy-code-for-removing-response.

Competing interests

The authors declare no competing interests.

References

Ajluni, T., Everett, D., Linn, T., Mink, R., Willcockson, W., and Wood, J. OSIRIS-REx, returning the asteroid sample. In *2015 IEEE aerospace conference*, pages 1–15. IEEE, 2015. doi: 10.1109/AERO.2015.7118988.

Allander, K. K. and Berger, D. L. Seismic velocities and thicknesses of alluvial deposits along Baker Creek in the Great Basin National Park, East-Central Nevada. *Technical Report, U. S. Geological Survey*, 2009. doi: https://doi.org/10.3133/ofr20091174.

Ben-Menahem, A. and Singh, S. J. *Seismic waves and sources*. Springer Science & Business Media, 1981. doi: https://doi.org/10.1007/978-1-4612-5856-8.

Bishop, J. W., Fee, D., Modrak, R., Tape, C., and Kim, K. Spectral element modeling of acoustic to seismic coupling over topography. *Journal of Geophysical Research: Solid Earth*, 127(1):e2021JB023142, 2022. doi: https://doi.org/10.1029/2021JB023142.

Busby, R. W. and Aderhold, K. The Alaska transportable array: As built. *Seismological Research Letters*, 91(6):3017–3027, 2020. doi: https://doi.org/10.1785/0220200154.

Ceplecha, Z., Borovička, J., Elford, W. G., ReVelle, D. O., Hawkes, R. L., Porubčan, V., and Šimek, M. Meteor phenomena and bodies. *Space Science Reviews*, 84:327–471, 1998. doi: https://doi.org/10.1023/A:1005069928850.

Chen, T., Larmat, C., Blom, P., and Zeiler, C. Seismoacoustic Analysis of the Large Surface Explosion Coupling Experiment Using a Large-N Seismic Array. *Bulletin of the Seismological Society of America*, 113(4):1692–1701, 2023. doi: https://doi.org/10.1785/0120220262.

Cook, J., Goforth, T., and Cook, R. Seismic and underwater responses to sonic boom. *The Journal of the Acoustical Society of America*, 51(2C):729–741, 1972. doi: https://doi.org/10.1121/1.1912906.

---

[2]https://www.iata.org/en/services/statistics/intelligence/co2-connect/
[3]https://www.epa.gov/energy/greenhouse-gas-equivalencies-calculator

Edwards, W. N., Eaton, D. W., McCausland, P. J., ReVelle, D. O., and Brown, P. G. Calibrating infrasonic to seismic coupling using the Stardust sample return capsule shockwave: Implications for seismic observations of meteors. *Journal of Geophysical Research*, 112(B10), 2007. doi: 10.1029/2006jb004621.

Edwards, W. N., Eaton, D. W., and Brown, P. G. Seismic observations of meteors: Coupling theory and observations. *Reviews of Geophysics*, 46(4), 2008. doi: https://doi.org/10.1029/2007RG000253.

Emmanuelli, A., Dragna, D., Ollivier, S., and Blanc-Benon, P. Characterization of topographic effects on sonic boom reflection by resolution of the Euler equations. *The Journal of the Acoustical Society of America*, 149(4):2437–2450, 2021. doi: https://doi.org/10.1121/10.0003816.

Fernando, B., Wójcicka, N., Froment, M., Maguire, R., Stähler, S. C., Rolland, L., Collins, G. S., Karatekin, O., Larmat, C., Sansom, E. K., et al. Listening for the landing: Seismic detections of Perseverance's arrival at Mars with InSight. *Earth and Space Science*, 8(4):e2020EA001585, 2021. doi: https://doi.org/10.1029/2020EA001585.

Fernando, B., Wójcicka, N., Maguire, R., Stähler, S. C., Stott, A. E., Ceylan, S., Charalambous, C., Clinton, J., Collins, G. S., Dahmen, N., et al. Seismic constraints from a Mars impact experiment using InSight and Perseverance. *Nature Astronomy*, 6(1):59–64, 2022. doi: https://doi.org/10.1038/s41550-021-01502-0.

Garcia, R. F., Daubar, I. J., Beucler, É., Posiolova, L. V., Collins, G. S., Lognonné, P., Rolland, L., Xu, Z., Wójcicka, N., Spiga, A., et al. Newly formed craters on Mars located using seismic and acoustic wave data from InSight. *Nature Geoscience*, 15(10):774–780, 2022. doi: https://doi.org/10.1038/s41561-022-01014-0.

Kenda, B., Drilleau, M., Garcia, R. F., Kawamura, T., Murdoch, N., Compaire, N., Lognonné, P., Spiga, A., Widmer-Schnidrig, R., Delage, P., Ansan, V., Vrettos, C., Rodriguez, S., Banerdt, W. B., Banfield, D., Antonangeli, D., Christensen, U., Mimoun, D., Mocquet, A., and Spohn, T. Subsurface Structure at the InSight Landing Site From Compliance Measurements by Seismic and Meteorological Experiments. *Journal of Geophysical Research: Planets*, 125(6), 2020. doi: 10.1029/2020je006387.

Kong, Q., Allen, R. M., Schreier, L., and Kwon, Y.-W. MyShake: A smartphone seismic network for earthquake early warning and beyond. *Science advances*, 2(2):e1501055, 2016. doi: https://doi.org/10.1126/sciadv.1501055.

Langston, C. A. Seismic ground motions from a bolide shock wave. *Journal of Geophysical Research: Solid Earth*, 109(B12), 2004. doi: https://doi.org/10.1029/2004JB003167.

Lauretta, D., Balram-Knutson, S., Beshore, E., Boynton, W., Drouet d'Aubigny, C., DellaGiustina, D., Enos, H., Golish, D., Hergenrother, C., Howell, E., et al. OSIRIS-REx: sample return from asteroid (101955) Bennu. *Space Science Reviews*, 212:925–984, 2017. doi: https://doi.org/10.1007/s11214-017-0405-1.

Lecocq, T., Hicks, S. P., Van Noten, K., Van Wijk, K., Koelemeijer, P., De Plaen, R. S., Massin, F., Hillers, G., Anthony, R. E., Apoloner, M.-T., et al. Global quieting of high-frequency seismic noise due to COVID-19 pandemic lockdown measures. *Science*, 369(6509):1338–1343, 2020. doi: https://doi.org/10.1126/science.abd2438.

Manconi, A., Coviello, V., Galletti, M., and Seifert, R. Monitoring rockfalls with the Raspberry Shake. *Earth Surface Dynamics*, 6(4):1219–1227, 2018. doi: https://doi.org/10.5194/esurf-6-1219-2018.

Matoza, R. S. and Fee, D. Infrasonic component of volcano-seismic eruption tremor. *Geophysical Research Letters*, 41(6):1964–1970, 2014. doi: https://doi.org/10.1002/2014GL059301.

Mikael, S. Establishment of the Ethiopian Seismic Monitoring Network. *Engineering Archive*, 2020. doi: https://doi.org/10.31224/osf.io/c6y8p.

Novoselov, A., Fuchs, F., and Bokelmann, G. Acoustic-to-seismic ground coupling: coupling efficiency and inferring near-surface properties. *Geophysical Journal International*, 223(1):144–160, 2020. doi: https://doi.org/10.1093/gji/ggaa304.

Pierce, A. D. and Maglieri, D. J. Effects of atmospheric irregularities on sonic-boom propagation. *The Journal of the Acoustical Society of America*, 51(2C):702–721, 1972. doi: https://doi.org/10.1121/1.1912904.

Plotkin, K. J. State of the art of sonic boom modeling. *The Journal of the Acoustical Society of America*, 111(1):530–536, 2002. doi: https://doi.org/10.1121/1.1379075.

ReVelle, D. and Edwards, W. Stardust—An artificial, low-velocity "meteor" fall and recovery: 15 January 2006. *Meteoritics & Planetary Science*, 42(2):271–299, 2007. doi: https://doi.org/10.1111/j.1945-5100.2007.tb00232.x.

ReVelle, D., Edwards, W., and Sandoval, T. Genesis—An artificial, low velocity "meteor" fall and recovery: September 8, 2004. *Meteoritics & Planetary Science*, 40(6):895–916, 2005. doi: https://doi.org/10.1111/j.1945-5100.2005.tb00162.x.

Sansom, E. K., Devillepoix, H. A., Yamamoto, M.-y., Abe, S., Nozawa, S., Towner, M. C., Cupák, M., Hiramatsu, Y., Kawamura, T., Fujita, K., et al. The scientific observation campaign of the Hayabusa-2 capsule re-entry. *Publications of the Astronomical Society of Japan*, 74(1):50–63, 2022. doi: https://doi.org/10.1093/pasj/psab109.

Silber, E. A., Bowman, D. C., and Albert, S. A Review of Infrasound and Seismic Observations of Sample Return Capsules Since the End of the Apollo Era in Anticipation of the OSIRIS-REx Arrival. *Atmosphere*, 14(10):1473, 2023. doi: https://doi.org/10.3390/atmos14101473.

Sorrells, G. G. A Preliminary Investigation into the Relationship between Long-Period Seismic Noise and Local Fluctuations in the Atmospheric Pressure Field. *Geophysical Journal of the Royal Astronomical Society*, 26(1-4):71–82, 1971. doi: 10.1111/j.1365-246X.1971.tb03383.x.

Wills, G., Nippress, A., Green, D. N., and Spence, P. J. Site-specific variations in air-to-ground coupled seismic arrivals from the 2012 October 16 explosion at Camp Minden, Louisiana, United States. *Geophysical Journal International*, 231(1):243–255, 2022. doi: https://doi.org/10.1093/gji/ggac184.

Winter, K., Lombardi, D., Diaz-Moreno, A., and Bainbridge, R. Monitoring icequakes in East Antarctica with the raspberry shake. *Seismological Research Letters*, 92(5):2736–2747, 2021. doi: https://doi.org/10.1785/0220200483.

Yamamoto, M.-y., Ishihara, Y., Hiramatsu, Y., Kitamura, K., Ueda, M., Shiba, Y., Furumoto, M., and Fujita, K. Detection of acoustic/infrasonic/seismic waves generated by hypersonic re-entry of the HAYABUSA capsule and fragmented parts of the spacecraft. *Publications of the Astronomical Society of Japan*, 63(5):971–978, 2011. doi: https://doi.org/10.1093/pasj/63.5.971.